SANDIA REPORT

SAND2015-8831
Unlimited Release
Printed October 2015

Towards Using Eshelby Calculations to Enhance Kinetic Model for Zirconium Hydride Precipitation

John A. Mitchell, Veena Tikare, Philippe F. Weck

Prepared by
Sandia National Laboratories
Albuquerque, New Mexico 87185 and Livermore, California 94550

Sandia National Laboratories is a multi-program laboratory managed and operated by Sandia Corporation, a wholly owned subsidiary of Lockheed Martin Corporation, for the U.S. Department of Energy's National Nuclear Security Administration under contract DE-AC04-94AL85000.

Sandia National Laboratories

Issued by Sandia National Laboratories, operated for the United States Department of Energy by Sandia Corporation.

Available to DOE and DOE contractors from
U.S. Department of Energy
Office of Scientific and Technical Information
P.O. Box 62
Oak Ridge, TN 37831

Telephone: (865) 576-8401
Facsimile: (865) 576-5728
E-Mail: reports@adonis.osti.gov
Online ordering: http://www.osti.gov/bridge

Available to the public from
U.S. Department of Commerce
National Technical Information Service
5285 Port Royal Rd
Springfield, VA 22161

Telephone: (800) 553-6847
Facsimile: (703) 605-6900
E-Mail: orders@ntis.fedworld.gov
Online ordering: http://www.ntis.gov/help/ordermethods.asp?loc=7-4-0#online

SAND2015-8831
Unlimited Release
Printed October 2015

Towards Using Eshelby Calculations to Enhance Kinetic Model for Zirconium Hydride Precipitation

John A. Mitchell & Veena Tikare
Multiscale Science

Philippe F. Weck
Storage and Transportation Technologies

Sandia National Laboratories
1515 Eubank SE
Albuquerque, NM 87185

Abstract

A c++ library (called *Eshelby*) was implemented in fiscal year 2015 based upon the formulas documented in this report. The library implements a generalized version of Eshelby's [1] inclusion problem. The library was written as a set of functions which can be called from another program; the principle intended use cases are kinetic models of precipitate formation in zirconium claddings where use of the *Eshelby* library provides needed elastic energy density calculations, as well as calculations of stress and strain in and around precipitates; it is intended that the library will be made open source. For isotropic inclusions in the form of oblate and prolate ellipsoids, the *Eshelby* library can be used for nearly any relevant/appropriate shape parameters to calculate strains, stresses and energy density at interior and exterior points. The *Eshelby* library uses a combination of analytical formulas and numerical routines making it very extensible. For example, the library can can easily be extended to include inclusions such as spheres since analytical expressions exist for the required elliptic integrals; similarly, general ellipsoids do not have analytical results for the required elliptic integrals but those integrals can be numerically evaluated and thus fit naturally into the Eshelby library. This report documents all formulas implemented in the *Eshelby* library and presents some demonstration calculations relevant to the intended application.

Acknowledgment

The authors would like to thank and gratefully acknowledge support from Ken Sorenson, Sylvia Saltzstein, and Remi Dingreville. The authors would also like to thank and gratefully acknowledge Chunfang Meng, currently a post-doc at MIT, for making his matlab implementation of the Eshelby approach available and for reviewing this report.

Contents

Appendix

List of Figures

List of Tables

1 Introduction

This report documents formulas for computing the elastic field in and around isotropic ellipsoidal shaped inclusions and serves as a mathematical guide for the c++ library implementation called *Eshelby*. The library is so named because its implementation follows the conceptual framework published in 1957 by John Eshelby [1]. However, many of the formulas presented here were subsequently developed and published later. Isotropic inclusions are very well documented in the book by Mura [2]. Also worth noting is the 2012 paper by Meng, Heltsley, and Pollard [3]; the present work most closely follows the conceptual framework presented by Meng, Heltsley and Pollard, but many of the detailed formulas were obtained from Mura. In addition, some formulas were also obtained analytically using Mathematica [4].

In the original work [1], Eshelby identified two kinds of problems: 1) the transformation problem (referred to here as the inclusion problem), which is the primary focus of this report, and 2) the inhomogeneity problem, which is an extension and generalization of the inclusion problem. The inhomogeneity problem is not documented here but may be a future addition to the Eshelby software library.

The Eshelby approach considers a solid material body $\mathscr{D} \subseteq \mathbb{R}^3$ and a finite sub-region $\Omega \subset \mathscr{D}$; a schematic is shown in Figure 1. The sub-region Ω undergoes an in-elastic transformation/deformation but because of the constraining/surrounding material an elastic field is induced in the body $\mathscr{D}$. The in-elastic transformation on Ω is referred to as an eigenstrain and when the body $\mathscr{D}$ and Ω are composed of the same material, Ω is referred to as an inclusion and the region outside $\mathscr{D}/\Omega$ is referred to as the matrix. The eigenstrain is non-zero in the inclusion and zero in the matrix. The Eshelby problem is to determine the displacements, strain, and stress fields in both the matrix and inclusion due to eigenstrains on the inclusion. Eshelby proposed a novel approach to solve for the induced elastic field. The Eshelby solution for ellipsoidal shaped inclusions is briefly introduced and described in this section of the report.

The concept of eigenstrain used in this report is quite general. Eigenstrains are in-elastic deformations on the inclusion that can arise from a variety of physical processes such as thermal expansion, precipitate formation or plastic deformations. Eigenstrains, denoted by ε^*_{ij}, give rise to eigenstresses σ_{ij}. When the body $\mathscr{D}$ is free of any other forces or surface constraints, eigenstresses are self-equilibriated internal stresses in $\mathscr{D}$ which arise due to the incompatibility of the in-elastic eigenstrains.

The remainder of the report is briefly outlined. The Eshelby approach to the inclusion problem is introduced in Section 2; this section includes an outline of the original conceptual development given by Eshelby but in a more generalized form that incorporates computation of elastic fields external to the inclusion; importantly, Section 2 contains definitions for the elliptic $I-$integrals which must be evaluated. Section 3 describes the approach used for evaluation of the $I-$integrals with a focus towards ultimately evaluating the Eshelby tensor – this discussion is relevant to any ellipsoidal shape; Section 3 concludes with analytical details related to evaluation of the $I-$integrals for oblate and prolate ellipsoids. The intended application of the Eshelby calculation is computation of the elastic field in an around inclusions – this is described in Section 4 with a focus on

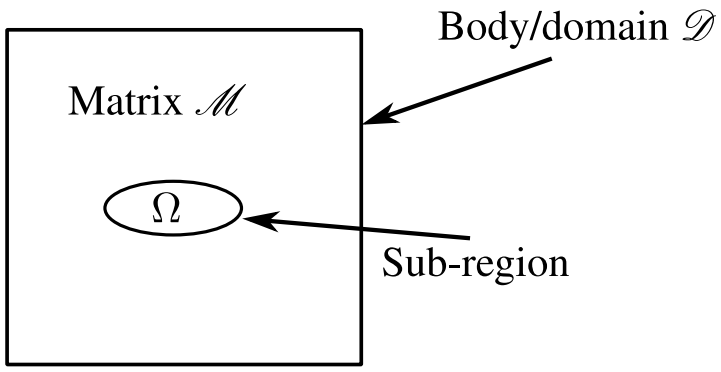

Figure 1: Schematic of body $\mathscr{D}$, inclusion Ω, and matrix $\mathscr{M}$.

development of formulas for elastic energy density; these formulas are relatively general and applicable to many simultaneous inclusions although that aspect is not emphasized; however, the case of two simultaneous inclusions is included. Section 4 also includes calculation of energy density when there co-exists an inclusion along with a state of stress/strain due to applied surface loads in the far field. Section 5 includes demonstration calculations using the Eshelby library. The included calculations do not fully cover all aspects of the Eshelby library application interface but they do demonstrate the power of the *Eshelby* library to resolve very complex fields at the matrix/inclusion interface. Note that the included appendices are relevant to Section 3 and provide additional details needed for evaluation of the Eshelby tensor.

2 Introduction to Eshelby Approach and Concepts

2.1 The Eshelby inclusion problem

Eshelby proposed a solution to the inclusion problem based upon a thought experiment consisting of the following assumptions and conceptual steps.

2.1.1 Assumptions

1. For a point $\mathbf{x} \in \mathscr{D}$, the total strain $\varepsilon_{ij}(\mathbf{x})$ is obtained by the additive decomposition of the in-elastic eigenstrain $\varepsilon^*_{ij}(\mathbf{x})$ with the elastic strain $e_{ij}(\mathbf{x})$

$$\varepsilon_{ij} = e_{ij} + \varepsilon^*_{ij}, \tag{1}$$

   where ε_{ij}, e_{ij}, ε^*_{ij} are assumed to be infinitesimal. For notation purposes, the positional dependence upon $\mathbf{x}$ may be omitted in the notation now and then.

2. Assuming linearity and using the superposition principle for linearized elasticity, a Green's function is used to calculate the displacement at an observation point $\mathbf{x} \in \mathscr{D}$ due to an applied force at a different point $\mathbf{x}' \in \mathscr{D}$.

3. The eigenstrains $\varepsilon^*_{mn}(\mathbf{x}')$ for $\mathbf{x}' \in \Omega$ are taken as uniform/constant on Ω and hence independent of $\mathbf{x}'$.

4. In-elastic eigenstrains $\varepsilon^*_{mn}(\mathbf{x}') = 0$ for points $\mathbf{x}' \in \mathscr{M}$ (outside of inclusion Ω). Relatedly, for inclusion type problems, where it is assumed the matrix and inclusion have the same elastic moduli C_{ijkl}, the superposition principle justifies taking Ω as an aggregrate of inclusions; the elastic field at any particular point is then the superposition of the fields due to each inclusion in the collection.

2.1.2 Thought experiment

1. Remove/cut the inclusion Ω from $\mathscr{D}$ leaving a hole in the shape of Ω; the remaining matrix material $\mathscr{D}/\Omega$ retains its original shape.

2. Because Ω has been removed, it can freely change shape due to the in-elastic transformation; without the constraint of the surrounding material, Ω is stress free. For points $\mathbf{x} \in \Omega$,

$$\sigma_{ij}(\mathbf{x}) = C_{ijkl} e_{kl}(\mathbf{x}) = C_{ijkl}(\varepsilon_{ij}(\mathbf{x}) - \varepsilon^*_{mn}(\mathbf{x})) = 0 \implies \varepsilon_{kl}(\mathbf{x}) = \varepsilon^*_{kl}(\mathbf{x}) \tag{2}$$

3. Apply a traction vector $\mathbf{t}$ to the surface $\partial\Omega$ of the removed volume Ω (inclusion) that returns Ω to its original undeformed shape and then insert Ω back into its original position.

Rejoin/weld the matrix material and inclusion across the cut. At this stage, the matrix $\mathscr{D}/\Omega$ is stress-free and un-deformed and is as if nothing has changed; the inclusion Ω is also un-deformed ($\varepsilon_{kl} = 0$) although it is not stress free due to the applied traction $\mathbf{t}$. The applied traction is given as

$$\mathbf{t} = \sigma \cdot \hat{n}, \tag{3}$$

where $\hat{n}$ is the unit normal pointing outward from the surface of the inclusion Ω, and σ denotes the tensor representation of the stress tensor components σ_{ij}. At this stage, for points $\mathbf{x} \in \Omega$,

$$\varepsilon_{kl}(\mathbf{x}) = 0 \implies \sigma_{ij}(\mathbf{x}) = C_{ijkl} e_{kl}(\mathbf{x}) = -C_{ijkl}\varepsilon^*_{kl}(\mathbf{x}). \tag{4}$$

4. The unknown elastic field in and around the inclusion is found by removing the applied traction vector $\mathbf{t}$; this is accomplished by applying an equal and opposite traction on the imaginary cut surface $\partial\Omega$ which effectively cancels and removes $\mathbf{t}$ leaving the original problem. However, because $\mathbf{t}$ is known and given by (3), the thought experiment gives way to a solution for the elastic field expressed in terms of a Green's function for an elastic body; the strain field is given by [2]

$$\varepsilon_{ij}(\mathbf{x}) = -\frac{1}{2}\int_\Omega C_{klmn}\varepsilon^*_{mn}(\mathbf{x}')\{G_{ik,lj}(\mathbf{x}-\mathbf{x}') + G_{jk,li}(\mathbf{x}-\mathbf{x}')\}d\mathbf{x}',$$

where $G_{ij}(\mathbf{x}-\mathbf{x}')$ denotes the Green's function. Physically, $G_{ij}(\mathbf{x}-\mathbf{x}')$ is the displacement component u_i at $\mathbf{x}$ for a unit point force component 1_j applied at $\mathbf{x}'$. Using assumption 3 above, $\varepsilon^*_{mn}(\mathbf{x}') = \varepsilon^*_{mn}$ can be brought outside the integral

$$\varepsilon_{ij}(\mathbf{x}) = -\frac{1}{2}C_{klmn}\varepsilon^*_{mn}\int_\Omega \{G_{ik,lj}(\mathbf{x}-\mathbf{x}') + G_{jk,li}(\mathbf{x}-\mathbf{x}')\}d\mathbf{x}'. \tag{5}$$

Because eigenstrains ε^*_{mn} vanish outside the inclusion (see assumption 4 above), the range of integration is conveniently limited to Ω. The integral in (5) is the starting point for ellipsoidal shaped inclusions Ω; under these conditions, Eshelby showed that components of both stress and strain are constant/uniform within the inclusion Ω. For isotropic materials, the Green's function in (5) is given by

$$G_{ij}(\mathbf{x}-\mathbf{x}') = \frac{1}{4\pi\mu}\frac{\delta_{ij}}{|\mathbf{x}-\mathbf{x}'|} - \frac{1}{16\pi\mu(1-\nu)}\frac{\partial^2}{\partial x_i \partial x_j}|\mathbf{x}-\mathbf{x}'|, \tag{6}$$

where μ and ν denote the shear modulus and Poisson ratio respectively.

2.2 Ellipsoidal shaped inclusions

In this section, mathematical formulas used to evaluate the elastic field inside and outside ellipsoidal shaped inclusions are presented. Eshelby [1] provided the original conceptual outline for evaluation of the elastic field with a focus for interior points (points within the inclusion); using the same conceptual framework, formulas for exterior points (outside of the inclusion) were later

developed and published. The formulas and notation given here closely follow the very high quality documentation given by Mura [2]; these formulas are quite detailed and especially difficult to obtain; generally, formulas are presented for purposes of documenting the evaluation software and only developed/derived as required for numerical evaluation. Formulas for generic ellipsoidal shaped inclusions are presented while shape specific details, such as formulas for spherical, prolate, and oblate ellipsoids, are given in a subsequent section.

An ellipsoid is described by the following equation

$$\frac{x_1^2}{a_1^2}+\frac{x_2^2}{a_2^2}+\frac{x_3^2}{a_3^2}=1, \tag{7}$$

where a_1, a_2, a_3 denote the ellipsoid dimensions along x_1, x_2, x_3 Cartesian coordinate axes respectively; the volume of the ellipsoid is $V=\frac{4\pi}{3}a_1a_2a_3$.

A point $\mathbf{x}\in\mathscr{D}$ defined by its Cartesian components (x_1,x_2,x_3) is an interior point when

$$\frac{x_1^2}{a_1^2}+\frac{x_2^2}{a_2^2}+\frac{x_3^2}{a_3^2}<1, \tag{8}$$

otherwise it is called at exterior point.

2.2.1 Eshelby tensor for isotropic materials

For a point $\mathbf{x}\in\mathscr{D}$, the Eshelby tensor $D_{ijkl}(\mathbf{x})$ linearly relates the eigenstrains ε^*_{kl} to strain $\varepsilon_{ij}(\mathbf{x})$ (see (1))

$$\varepsilon_{ij}(\mathbf{x})=D_{ijkl}(\mathbf{x})\varepsilon^*_{kl}. \tag{9}$$

For both interior and exterior points, $D_{ijkl}(\mathbf{x})$ is obtained by substituting (6) into (5) and can be expressed as

$$8\pi(1-\nu)D_{ijkl}(\mathbf{x})=\psi_{,ijkl}-2\nu\delta_{kl}\phi_{,ij}-(1-\nu)[\phi_{,kj}\delta_{il}+\phi_{,ki}\delta_{jl}+\phi_{,lj}\delta_{ik}+\phi_{,li}\delta_{jk}], \tag{10}$$

where $\phi(\mathbf{x})$ and $\psi(\mathbf{x})$ are given by the following integrals

$$\phi(\mathbf{x})=\int_\Omega\frac{d\mathbf{x}'}{|\mathbf{x}-\mathbf{x}'|},\quad \psi(\mathbf{x})=\int_\Omega|\mathbf{x}-\mathbf{x}'|d\mathbf{x}'. \tag{11}$$

When the inclusion is an ellipsoid, $\phi(\mathbf{x})$ and $\psi(\mathbf{x})$ are expressed using the following integrals (later referred to as the I-integrals)

$$\begin{aligned}
I(\lambda)&=2\pi a_1a_2a_3\int_\lambda^\infty\frac{ds}{\Delta(s)}\\
I_i(\lambda)&=2\pi a_1a_2a_3\int_\lambda^\infty\frac{ds}{(a_i^2+s)\Delta(s)}\\
I_{ij}(\lambda)&=2\pi a_1a_2a_3\int_\lambda^\infty\frac{ds}{(a_i^2+s)(a_j^2+s)\Delta(s)},
\end{aligned} \tag{12}$$

where

$$\Delta(s) = \{(a_1^2+s)(a_2^2+s)(a_3^2+s)\}^{1/2}. \tag{13}$$

Note that $I_{ij}(\lambda) = I_{ji}(\lambda)$. For exterior points $\mathbf{x} \in \mathscr{M}$, λ is the largest possible root of the equation

$$\frac{x_i x_i}{a_I^2+\lambda} = \frac{x_1^2}{a_1^2+\lambda} + \frac{x_2^2}{a_2^2+\lambda} + \frac{x_3^2}{a_3^2+\lambda} = 1, \tag{14}$$

otherwise $\lambda = 0$ when $\mathbf{x} \in \Omega$ (interior point). The above equation illustrates a slightly unconventional notation mixing upper and lower case indices. Repeated lower case indices imply the usual summation convention while upper case indices take on the same number as the corresponding lower case but are not summed.

The potential functions $\phi(\mathbf{x})$ and $\psi(\mathbf{x})$ are expressed using the I-integrals (12)

$$\begin{aligned}
\phi(\mathbf{x}) &= \frac{1}{2}[I(\lambda) - x_n x_n I_N(\lambda)] \\
\psi_{,i}(\mathbf{x}) &= \frac{1}{2} x_i \{I(\lambda) - x_n x_n I_N(\lambda) - a_I^2 [I_I(\lambda) - x_n x_n I_{IN}(\lambda)]\}.
\end{aligned} \tag{15}$$

Using (10) and (19), the final form of the Eshelby tensor is expressed in terms of I-integrals and partial derivatives of I-integrals,

$$\begin{aligned}
8\pi(1-\nu)D_{ijkl}(\mathbf{x}) = {} & 8\pi(1-\nu)S_{ijkl}(\lambda) + 2\nu\delta_{kl}x_i I_{I,j}(\lambda) \\
& + (1-\nu)\{\delta_{il}x_k I_{K,j}(\lambda) + \delta_{jl}x_k I_{K,i}(\lambda) + \delta_{ik}x_l I_{L,j}(\lambda) + \delta_{jk}x_l I_{L,i}(\lambda)\} \\
& - \delta_{ij}x_k\{I_{K,l}(\lambda) - a_I^2 I_{KI,l}(\lambda)\} - (\delta_{ik}x_j + \delta_{jk}x_i)\{I_{J,l}(\lambda) - a_I^2 I_{IJ,l}(\lambda)\} \\
& - (\delta_{il}x_j + \delta_{jl}x_i)\{I_{J,k}(\lambda) - a_I^2 I_{IJ,k}(\lambda)\} - x_i x_j\{I_{J,lk}(\lambda) - a_I^2 I_{IJ,lk}(\lambda)\}
\end{aligned} \tag{16}$$

where

$$\begin{aligned}
8\pi(1-\nu)S_{ijkl}(\lambda) = {} & \delta_{ij}\delta_{kl}\{2\nu I_I(\lambda) - I_K(\lambda) + a_I^2 I_{IK}(\lambda)\} \\
& + (\delta_{ik}\delta_{jl} + \delta_{jk}\delta_{il})\{a_I^2 I_{IJ}(\lambda) - I_J(\lambda) + (1-\nu)\{I_K(\lambda) + I_L(\lambda)\}\}
\end{aligned} \tag{17}$$

Details needed to arrive at the terms in expressions (16) and (17) are given in Appendix 1; details needed for computer evaluation of these expressions are given in Section 3. It is important to note that for constant eigenstrains, Eshelby [1] showed that the resulting elastic field (both stresses and strains) is uniform for interior points. Recall that $\lambda = 0$ for interior points (see (14)). The consequence of Eshelby's result is that for interior points $\mathbf{x} \in \Omega$, partial derivatives of the I-integrals vanish and therefore $D_{ijkl}(\mathbf{x}) = S_{ijkl}(0)$.

3 Evaluating Eshelby Tensor on Ellipsoidal Inclusions

In this section, expressions for $D_{ijkl}(\mathbf{x})$ and $S_{ijkl}(\lambda)$ in (16) and (17) respectively, are further developed for specific ellipsoidal shapes: prolate and oblate; these formulas ultimately depend upon the $I-$integrals in (12). The numerical implementation documented here uses several different strategies for evaluation of these integrals. The key strategies used are enumerated below.

1. Although it does not always work, whenever possible, use mathematica [4] to evaluate difficult integrals. For the oblate ellipsoid, new expressions, not known to be published elsewhere, were obtained using mathematica. Apparently, the new expressions are mathematically equivalent to the expressions given by Mura [2]. The new expressions are given in Section 3.2 describing the oblate shape.

2. Eshelby [1] original published relations between the integrals for computation of S_{ijkl} at interior points. Mura [2] and Meng [3] published relations between the integrals for both interior and exterior points. These relations are very useful but must be used with care to avoid division by zero in cases when $a_i = a_j$ $(i \neq j)$. Even in these cases, the relations still yield necessary information for evaluation of all the integrals. These relations are:

$$\begin{aligned} I_1(\lambda)+I_2(\lambda)+I_3(\lambda) &= \frac{4\pi a_1 a_2 a_3}{\Delta(\lambda)} \\ I_{ij}(\lambda) &= -\frac{I_i(\lambda)-I_j(\lambda)}{a_i^2-a_j^2} \\ I_{ii}(\lambda) &= \frac{4\pi a_1 a_2 a_3}{3(a_i^2+\lambda)\Delta(\lambda)} - \frac{1}{3}\sum_{j\neq i} I_{ij}(\lambda) \end{aligned} \tag{18}$$

3. Use the GNU Scientific Library (GSL) [5] for root finding (see (14)), and numerical evaluation of the I-integrals (12). To that end, the following standardized elliptic integrals are used in the numerical evaluation of the I-integrals (12).

$$\begin{aligned} F(\theta(\lambda),k) &= \int_0^{\theta(\lambda)} \frac{dw}{[1-k^2\sin^2(w)]^{\frac{1}{2}}} \\ E(\theta(\lambda),k) &= \int_0^{\theta(\lambda)} [1-k^2\sin^2(w)]^{\frac{1}{2}} dw \end{aligned} \tag{19}$$

4. Observe relations between the integrals when principal dimensions of an ellipsoid are equal. For example, this strategy is used for the prolate ellipsoid. Since $a_1 > a_2 = a_3$, inspection of the integrals (12) gives $I_2(\lambda) = I_3(\lambda)$.

Once values for the $I-$integrals are obtained, expressions for partial derivatives of the $I-$integrals can be evaluated using formulas given in Appendix 1; then, these values are substituted into expressions for $D_{ijkl}(\mathbf{x})$ and $S_{ijkl}(\lambda)$ given in (16) and (17).

3.1 Prolate ellipsoidal inclusion

Evaluation of the Eshelby tensor for prolate ellipsoids is described in this section. Only details relevant to the prolate shape are given here. In this case, $a_1 > a_2 = a_3$ and nearly all of the strategies enumerated above are used. The following description also sequentially follows the order used for the numerical evaluation of the Eshelby tensor.

The root λ of (14) is evaluated using the GSL [5] library. Since $a_1 > a_2 = a_3$, the integral for I_1 in (12) is expressed using standard elliptic integrals [3] ($F(\theta(\lambda),k)$ and $E(\theta(\lambda),k)$ below) which can be evaluated using the GSL library

$$I_1(\lambda) = \frac{4\pi a_1 a_2 a_3}{(a_1^2 - a_2^2)(a_1^2 - a_3^2)^{\frac{1}{2}}}[F(\theta(\lambda),k) - E(\theta(\lambda),k)], \tag{20}$$

where $E(\theta(\lambda),k)$ and $F(\theta(\lambda),k)$ are defined in 19, and

$$\theta(\lambda) = \arcsin\left[\left(\frac{a_1^2 - a_3^2}{a_2^2 + \lambda}\right)^{\frac{1}{2}}\right]$$
$$k = \sqrt{\frac{a_1^2 - a_2^2}{a_1^2 - a_3^2}}.$$

At this stage, it assumed that $I_1(\lambda)$ has been evaluated. Because $a_2 = a_3$, strategy item 4 implies $I_2(\lambda) = I_3(\lambda)$; using strategy item 2 gives

$$I_2(\lambda) = \frac{1}{2}[4\pi - I_1(\lambda)] = I_3(\lambda). \tag{21}$$

Given numerical values for $I_j(\lambda)$, the second relation in strategy item 2 is used to evaluate $I_{12}(\lambda)$

$$I_{12}(\lambda) = -\frac{I_1(\lambda) - I_2(\lambda)}{a_1^2 - a_2^2}. \tag{22}$$

Using $a_2 = a_3$ implies that $I_{12}(\lambda) = I_{13}(\lambda)$, and $I_{22}(\lambda) = I_{23}(\lambda) = I_{33}(\lambda)$; using these conditions along with the third strategy item 2 gives

$$I_{22}(\lambda) = \frac{1}{4}\left[\frac{4\pi a_1 a_2 a_3}{(a_2^2 + \lambda)\Delta(\lambda)} - I_{12}(\lambda)\right]. \tag{23}$$

3.2 Oblate ellipsoidal inclusion

Evaluation of the Eshelby tensor for oblate ellipsoids is described in this section. Only details relevant to the oblate shape are given here. In this case, $a_1 = a_2 > a_3$ and nearly all of the strategies enumerated above are used. The following description also sequentially follows the order used for the numerical evaluation of the Eshelby tensor.

Using mathematica [4], $I_3(\lambda)$ was analytically obtained

$$I_3(\lambda) = 4\pi a_1^2 a_3 \left[\frac{1}{(a_1^2 - a_3^2)\sqrt{a_3^2+\lambda}} - \frac{\arccos\sqrt{\frac{a_3^2+\lambda}{a_1^2+\lambda}}}{((a_1-a_3)(a_1+a_3))^{\frac{3}{2}}} \right]. \tag{24}$$

Using strategy item 2 provides the following relation

$$I_2(\lambda) = \frac{4\pi a_1 a_2 a_3}{\Delta(\lambda)} - I_1(\lambda) - I_3(\lambda). \tag{25}$$

Since $a_1 = a_2$, strategy item 4 means that $I_1(\lambda) = I_2(\lambda)$; substituting this relation into (25) and solving for $I_2(\lambda)$ expressed using the known value for $I_3(\lambda)$ in (24) gives

$$I_2(\lambda) = \frac{4\pi a_1 a_2 a_3}{2\Delta(\lambda)} - \frac{1}{2} I_3(\lambda) = I_1(\lambda). \tag{26}$$

Since $a_1 = a_2$, inspection of the 3rd integral in (12) means that $I_{13}(\lambda) = I_{23}(\lambda)$; then the 2nd relation in strategy item 2 provides a value.

$$I_{13}(\lambda) = I_{23}(\lambda) = -\left[\frac{I_2(\lambda) - I_3(\lambda)}{a_2^2 - a_3^2} \right] \tag{27}$$

Since $a_1 = a_2$, the 3rd integral in (12) means that $I_{11}(\lambda) = I_{12}(\lambda) = I_{22}(\lambda)$; using the 3rd relation in strategy item 2 gives

$$I_{12}(\lambda) = I_{22}(\lambda) = I_{11}(\lambda) = \frac{1}{4}\left[\frac{4\pi a_1 a_2 a_3}{(a_1^2+\lambda)\Delta(\lambda)} - I_{13}(\lambda) \right] \tag{28}$$

and

$$I_{33}(\lambda) = \frac{1}{3}\left[\frac{4\pi a_1 a_2 a_3}{(a_3^2+\lambda)\Delta(\lambda)} - (I_{13}(\lambda) + I_{23}(\lambda)) \right]. \tag{29}$$

4 Evaluating Elastic Field on Ellipsoidal Isotropic Inclusions

In this section, the elastic field in an around an inclusion Ω, due to in-elastic eigenstrain components ε^*_{kl}, is evaluated; this includes development of formulas for elastic strain, stress, and energy, all of which are evaluated for both interior and exterior points of an ellipsoidal inclusion. Eigenstrains are zero outside the inclusion and assumed to be non-zero and spatially uniform/constant on the inclusion; the matrix and inclusion have the same isotropic elastic moduli. Note that some formulas presented are more generally valid for inclusions of any shape but the focus here is ellipsoidal shaped inclusions.

Once the Eshelby tensor $D_{ijkl}(\mathbf{x})$ is calculated for a point $\mathbf{x} \in \mathscr{D}$, components of the total strain $\varepsilon_{ij}(\mathbf{x})$ are calculated

$$\varepsilon_{ij}(\mathbf{x}) = D_{ijkl}(\mathbf{x})\varepsilon^*_{kl}, \tag{30}$$

where ε^*_{kl} is the constant valued eigenstrain on the inclusion; since $D_{ijkl}(\mathbf{x})$ carries the dependence of the observation point $\mathbf{x}$, the formula is valid for interior and exterior points. Assuming the additive decomposition (see (1)) of strains, components of the elastic strain tensor are computed

$$e_{ij}(\mathbf{x}) = \varepsilon_{ij}(\mathbf{x}) - \varepsilon^*_{ij}(\mathbf{x}), \tag{31}$$

where spatial dependence of the eigenstrains on $\mathbf{x}$ is used to emphasize that for $\mathbf{x} \in \Omega$, eigenstrains are nonzero and uniform/constant while for $\mathbf{x} \in \mathscr{M}$ eigenstrains are zero; this latter condition must be adhered to when evaluating the elastic strain.

Using the elastic strain components $e_{ij}(\mathbf{x})$ above, stress components for points interior or exterior to the isotropic inclusion are evaluated

$$\sigma_{ij}(\mathbf{x}) = \lambda e_{kk}(\mathbf{x})\delta_{ij} + 2\mu e_{ij}(\mathbf{x}), \tag{32}$$

where λ and μ denote isotropic material moduli.

4.1 Elastic energy

The total elastic energy W^* is given as

$$W^* = \frac{1}{2}\int_{\mathscr{D}} \sigma_{ij}(\mathbf{x})e_{ij}(\mathbf{x})dv. \tag{33}$$

The linearized strain tensor $\varepsilon_{ij}(\mathbf{x})$ evaluated in (30) also satisfies the strain-displacement relationship

$$\varepsilon_{ij}(\mathbf{x}) = \frac{1}{2}[u_{i,j}(\mathbf{x}) + u_{j,i}(\mathbf{x})]. \tag{34}$$

Using (31), (34), and symmetry of the stress tensor, the total elastic energy becomes

$$W^* = \frac{1}{2}\int_{\mathscr{D}} \sigma_{ij}(\mathbf{x})[u_{i,j}(\mathbf{x}) - \varepsilon^*_{ij}(\mathbf{x})]dv.$$

Integrating the first term in W^* by parts gives

$$\int_{\partial\mathscr{D}} \sigma_{ij}(\mathbf{x})u_i(\mathbf{x})n_j(\mathbf{x})dS = \int_{\mathscr{D}} \sigma_{ij,j}(\mathbf{x})u_i(\mathbf{x})dv + \int_{\mathscr{D}} \sigma_{ij}(\mathbf{x})u_{i,j}(\mathbf{x})dv = 0, \tag{35}$$

where the above equates to zero based upon the following assumptions.

- Body $\mathscr{D}$ is traction free; therefore $\sigma_{ij}(\mathbf{x})u_i(\mathbf{x})n_j(\mathbf{x}) = 0$ on $\partial\mathscr{D}$.
- Eigenstresses σ_{ij} are self-equilibriated; therefore $\sigma_{ij,j}(\mathbf{x}) = 0$

The total elastic energy becomes

$$W^* = -\frac{1}{2}\int_{\mathscr{D}} \sigma_{ij}(\mathbf{x})\varepsilon^*_{ij}(\mathbf{x})dv = -\frac{1}{2}\int_{\Omega} \sigma_{ij}(\mathbf{x})\varepsilon^*_{ij}dv = -\frac{1}{2}V\sigma^I_{ij}\varepsilon^*_{ij}, \tag{36}$$

where the domain of integration is reduced from $\mathscr{D}$ to Ω since ε^*_{ij} is zero outside of the inclusion Ω; superscript I denotes inclusion, and V denotes the inclusion volume. Note that Eshelby [1] showed σ^I_{ij} is uniform/constant on the inclusion which permits bringing it outside the integral.

The total elastic strain energy is stored in the matrix and the inclusion.

$$W^* = W^I + W^M, \tag{37}$$

where superscripts I and M denote inclusion and matrix respectively. The elastic energy stored in the inclusion is given as

$$W^I = \frac{1}{2}\int_{\Omega} \sigma^I_{ij}e^I_{ij}dv = \frac{1}{2}\int_{\Omega} \sigma^I_{ij}(\varepsilon^I_{ij} - \varepsilon^*_{ij})dv = \frac{1}{2}V\sigma^I_{ij}(\varepsilon^I_{ij} - \varepsilon^*_{ij}), \tag{38}$$

where stress σ^I_{ij} and strain ε^I_{ij} are constant on the inclusion. The elastic energy stored in the matrix is found by equating (36) with (38) and solving for W^M

$$W^M = -\frac{1}{2}\int_{\Omega} \sigma^I_{ij}\varepsilon^I_{ij}dv = -\frac{1}{2}V\sigma^I_{ij}\varepsilon^I_{ij}. \tag{39}$$

4.2 Elastic energy of two inclusions

Using principles developed in the previous section, the elastic energy in and around two inclusions is developed. The analysis here assumes that the two inclusions neither touch or overlap. It is necessary to invoke the superposition assumption (item 4) described in Section 2.1.1; since elastic moduli are taken as equivalent for both matrix and inclusions, displacements, stresses and strains at a point are a superposition of those due to eigenstrains on each inclusion. Due to the additional

complexity of a second inclusion, the notation is enhanced to include eigenstrains $\varepsilon^{\mathrm{k}}_{ij}$ on the k^{th} inclusion for $k = 1,2$; eigenstresses due to eigenstrains on the k^{th} inclusion are denoted by σ^{k}_{ij}. Note that $\varepsilon^1_{ij} = 0$ on $\mathscr{D}/\Omega_1$ and $\varepsilon^2_{ij} = 0$ on $\mathscr{D}/\Omega_2$; using this and (36), the total elastic energy for two inclusions is give as

$$W^* = -\frac{1}{2}\int_{\Omega_1}[\sigma^1_{ij}(\mathbf{x}) + \sigma^2_{ij}(\mathbf{x})]\varepsilon^1_{ij}(\mathbf{x})dv - \frac{1}{2}\int_{\Omega_1}[\sigma^1_{ij}(\mathbf{x}) + \sigma^2_{ij}(\mathbf{x})]\varepsilon^2_{ij}(\mathbf{x})dv. \tag{40}$$

The above total elastic energy can be substantially simplified. Mura [2] shows that

$$\begin{aligned}\int_{\Omega_1}\sigma^2_{ij}(\mathbf{x})\varepsilon^1_{ij}(\mathbf{x})dv &= -\int_{\mathscr{D}}\sigma^2_{ij}(\mathbf{x})e^1_{ij}(\mathbf{x})dv\\ \int_{\Omega_2}\sigma^1_{ij}(\mathbf{x})\varepsilon^2_{ij}(\mathbf{x})dv &= -\int_{\mathscr{D}}\sigma^1_{ij}(\mathbf{x})e^2_{ij}(\mathbf{x})dv.\end{aligned} \tag{41}$$

Using these results and $\sigma^2_{ij}e^1_{kl} = C_{ijkl}e^2_{kl}e^1_{ij} = \sigma^1_{kl}e^2_{kl}$, the total elastic energy is simplified to

$$W^* = -\frac{1}{2}\int_{\Omega_1}\sigma^1_{ij}(\mathbf{x})\varepsilon^1_{ij}(\mathbf{x})dv - \frac{1}{2}\int_{\Omega_2}\sigma^2_{ij}(\mathbf{x})\varepsilon^2_{ij}(\mathbf{x})dv - \int_{\Omega_1}\sigma^2_{ij}(\mathbf{x})\varepsilon^1_{ij}(\mathbf{x})dv. \tag{42}$$

From a numerical implementation point of view, (42) is convenient for computation of the total elastic energy; the first two terms are simply the total elastic energy of each inclusion in the absence of the other; the last term is the so-called interaction energy. The first two terms can be evaluated directly using (36) while the last term requires integration. The intended application for the present work requires the total energy density $w*$ which simplifies the calculation (removes the integral) but requires a slightly different form since it is needed for each point $\mathbf{x}$. Using the relations (41), and $\sigma^2_{ij}e^1_{kl} = \sigma^1_{kl}e^2_{kl}$, the following form of the total elastic energy is convenient for extracting the total elastic energy density $w^*(\mathbf{x})$

$$\begin{aligned}W^* =& -\frac{1}{2}\int_{\Omega_1}\sigma^1_{ij}(\mathbf{x})\varepsilon^1_{ij}(\mathbf{x})dv - \frac{1}{2}\int_{\Omega_2}\sigma^2_{ij}(\mathbf{x})\varepsilon^2_{ij}(\mathbf{x})dv - \int_{\Omega_1}\sigma^2_{ij}(\mathbf{x})\varepsilon^1_{ij}(\mathbf{x})dv\\ =&\frac{1}{2}\int_{\mathscr{D}}\sigma^1_{ij}(\mathbf{x})e^1_{ij}(\mathbf{x})dv + \frac{1}{2}\int_{\mathscr{D}}\sigma^2_{ij}(\mathbf{x})e^2_{ij}(\mathbf{x})dv + \int_{\mathscr{D}}\sigma^1_{ij}(\mathbf{x})e^2_{ij}(\mathbf{x})dv\\ =&\int_{\mathscr{D}}w^*(\mathbf{x})dv.\end{aligned} \tag{43}$$

In this form, the first two terms in the elastic energy density can be computed independently; the last term (interaction term) requires evaluation of the stress at a point $\mathbf{x}$ due to the inclusion on Ω_1 and evaluation of the elastic strain at $\mathbf{x}$ due to the inclusion on Ω_2 – these calculations are easily handled using the machinery described in Sections 2 and 3. Note that the interaction term is due to the coexistence of both inclusions.

4.3 Elastic energy of inclusion and applied tractions

In this section, a body containing inclusions on Ω is also subject to surface tractions. The intended use case is the application of tractions in the far field which induce a known or assumed state of uniform stress throughout the domain $\mathscr{D}$; this isn't a requirement but it simplifies practical application

of this theory as it doesn't require a separate boundary value problem to evaluate displacements u_i^o and strains $u_{i,j}^o$.

In the absence of inclusions, stresses and displacements due to surface tractions are denoted by σ_{ij}^o and u_i^o respectively. Eigenstrains ε_{ij}^* on Ω induce eigenstresses σ_{ij}; eigenstresses are self-equilibriated stresses on the body under zero loading conditions and therefore $\sigma_{ij}^o(\mathbf{x})[u_{i,j}^o(\mathbf{x}) + u_{i,j}(\mathbf{x})] = 0$. The total elastic energy due to the coexistence of both the applied tractions and inclusions Ω is given by the superposition principle and is a direct application of (33).

$$W^* = \frac{1}{2}\int_{\mathscr{D}} [\sigma_{ij}^o(\mathbf{x}) + \sigma_{ij}(\mathbf{x})][u_{i,j}^o(\mathbf{x}) + u_{i,j}(\mathbf{x}) - \varepsilon_{ij}^*(\mathbf{x})]dv.$$

The above expression for W^* is substantially simplified based upon the following analysis and relations.

- Eigenstresses σ_{ij} are self-equilibriated; since eigenstresses are induced by eigenstrains under zero traction conditions, integration by parts gives $\int_{\mathscr{D}} \sigma_{ij}(\mathbf{x})[u_{i,j}^o(\mathbf{x}) + u_{i,j}(\mathbf{x})]dv = 0$. Note also that this argument can be applied to $u_{i,j}^o$ separately from $u_{i,j}$; this is useful below for arriving at the total elastic energy density for an arbitrary point $\mathbf{x}$.

- Note that $\sigma_{ij}^o(\mathbf{x})[u_{i,j}(\mathbf{x}) - \varepsilon_{ij}^*] = C_{ijkl}u_{k,l}^o(\mathbf{x})[u_{i,j}(\mathbf{x}) - \varepsilon_{ij}^*] = u_{k,l}^o(\mathbf{x})\sigma_{kl}(\mathbf{x})$; in this form, the fact that σ_{kl} is an eigenstress means that $\int_{\mathscr{D}} \sigma_{ij}^o(\mathbf{x})[u_{i,j}(\mathbf{x}) - \varepsilon_{ij}^*]dv = 0$

Using the above relations, the total elastic energy W^* takes on the following simplified forms

$$\begin{aligned} W^* =& \frac{1}{2}\int_{\mathscr{D}} \sigma_{ij}^o(\mathbf{x})u_{i,j}^o(\mathbf{x})dv + \frac{1}{2}\int_{\mathscr{D}} \sigma_{ij}(\mathbf{x})[u_{i,j}(\mathbf{x}) - \varepsilon_{ij}^*]dv \\ =& \int_{\mathscr{D}} w^*(\mathbf{x})dv \\ =& \frac{1}{2}\int_{\mathscr{D}} \sigma_{ij}^o(\mathbf{x})u_{i,j}^o(\mathbf{x})dv - \frac{1}{2}\int_{\Omega} \sigma_{ij}(\mathbf{x})\varepsilon_{ij}^* dv. \end{aligned} \tag{44}$$

Identifying $w^*(\mathbf{x})$ is useful wherever energy density calculations are needed; when σ_{ij}^o is uniform and constant the first term in the energy density is easily evaluated. The second term arising from inclusions is obtained using the machinery documented in Sections 2 and 3; specifically, this term requires evaluation of the elastic strain and associated eigenstresses at a point $\mathbf{x}$ due to eigenstrains on the inclusion.

(a) Oblate (b) Prolate

Figure 2: Ellipsoids

Table 1: Demonstration calculations: fundamental units used.

Unit	Value
Mass	10^{-6} Kg = mg = milligram
Length	10^{-6} m = micron
Time	10^{-6} seconds

5 Demonstration Calculations

A c++ library (called *Eshelby*) was implemented based upon the formulas documented in this report. The library was written as a set of functions which can be called from another program. Although stress and energy calculations in and around precipitates may be useful in other contexts, the principle intended use cases for the *Eshelby* library are kinetic models of precipitate formation in zirconium claddings where use of the *Eshelby* library provides needed elastic energy density calculations. For oblate and prolate ellipsoidal inclusions, the *Eshelby* library can be used for nearly any relevant/appropriate shape parameters to calculate strains, stresses and energy density at interior and exterior points. The *Eshelby* library is implemented based upon the concept of a consistent set of units; for the calculations presented in this report, the fundamental set of units used are given in Table 1; derived units for stress and energy density are given in Table 5; unless otherwise stated, graphics presented here containing stress and energy density use these units.

5.1 Energy calculations around single inclusion

In this section, demonstration calculations are presented for both oblate and prolate shaped inclusions (see Figure 2). Size parameters, eigenstrains, and material moduli used in these calculations (see Tables 3 and 4) are roughly equal to those thought to occur in the zirconium claddings of spent nuclear fuel rods; isotropic moduli used are given in Table 2.

Table 2: Isotropic material moduli

Property	Value	Units
Young's modulus: E	95×10^{-3}	*Tera Pa*
Poisson's ratio: ν	.34	*dimensionless*

Table 3: Oblate ellipsoid parameters; see Figure (2a).

Property	Value	Units
Major axis: a_1	.5	*microns*
Major axis: a_2	.5	*microns*
Minor axis: a_3	.05	*microns*
ε_{11}	.0048	*dimensionless*
ε_{22}	.0048	*dimensionless*
ε_{33}	.0072	*dimensionless*
ε_{ij}, for $i \neq j$	0	*dimensionless*

Table 4: Prolate ellipsoid parameters; see Figure (2b).

Property	Value	Units
Major axis: a_1	.5	*microns*
Minor axis: a_2	.05	*microns*
Minor axis: a_3	.05	*microns*
ε_{11}	.0072	*dimensionless*
ε_{22}	.0048	*dimensionless*
ε_{33}	.0048	*dimensionless*
ε_{ij}, for $i \neq j$	0	*dimensionless*

Table 5: Derived units of stress and energy density; see Table 1; $\mu = 10^{-6}$.

Unit	Value
Force	Newtons
Stress	10^{12} Pascals = Tera Pa
Energy density	$\frac{\mu J}{(\mu m)^3}$ = micro Joules per cubic micron

Eshelby showed that stress and strain are uniform within isotropic ellipsoidal inclusions; it follows that the energy density within an inclusion is also constant. There is a discontinuity in energy density at the surface of the inclusion, and a fast decay with distance from the inclusion surface. The following two subsections illustrate these features for oblate and prolate inclusions.

The calculations presented here for the prolate case are not strictly analytical because the GNU Scientific Library (GSL) [5] was used to evaluate elliptic integrals introduced in Section 3. However, integrals were evaluated using error tolerances representing machine precision for 64-bit representation of floating point values and hence are representative of analytical results to machine precision.

5.1.1 Oblate

Energy density calculations for an oblate inclusion are shown in Figures 3 thru 5. Starting at $x_1 = x_2 = x_3 = 0$ and for fixed $x_2 = 0$, energy density is shown in Figure 3 as a function of x_1 for several fixed values of x_3; for $x_3 < 0.5$, each curve begins inside the inclusion where the energy density has a constant value – for these curves there is a value of x_1 where the triplet (x_1, x_2, x_3) exits the inclusion and the energy density has a discontinuity; note that the energy density rapidly decays with distance from the inclusion. The only other significant variation in energy density occurs at exterior points near and along the rim/edge of the inclusion; the curves in Figure 3 increase after the drop/discontinuity as x_1 approaches the rim/edge. The section plots in Figure 4 show a uniform/constant value for energy density at interior points and the zoomed view in Figure 5 shows the rise that occurs at exterior points near the rim/edge of the oblate precipitate; note that the bottom graphic in Figure 4 is a somewhat low-resolution depiction of the blue curve in Figure 3.

5.1.2 Prolate

Energy density calculations for a prolate inclusion are shown in Figures 6 thru 10. Starting at $x_1 = x_2 = x_3 = 0$ and for fixed $x_2 = 0$, energy density is shown in Figure 6 as a function of x_1 for several fixed values of x_3; for values $x_3 < 0.5$, each curve begins inside the inclusion where the energy density has a constant value – for these curves there is a value of x_1 where the triplet (x_1, x_2, x_3) exits the inclusion and the energy density has a discontinuity; similar plots are shown for energy density as a function of x_2 in Figures 7 and 8; these curves are similar to those seen in Figure 3 for the oblate inclusion; energy density is constant on the interior of the inclusion and rapidly decays with distance from the inclusion. One noticeable difference with the oblate case is the immediate drop (and no subsequent rise) at the surface of the inclusion; note that for the oblate inclusion, energy density rises before it decays to zero with distance from end – see Figure 3.

An image of the energy density on the cross-section of the prolate inclusion is shown in Figure 9; this graphic of the energy density in the $x_2 - x_3$ plane depicts the blue curve in Figure 8. The energy density of the prolate case in the $x_1 - x_3$ plane at $x_2 = 0$ is shown in Figure 10.

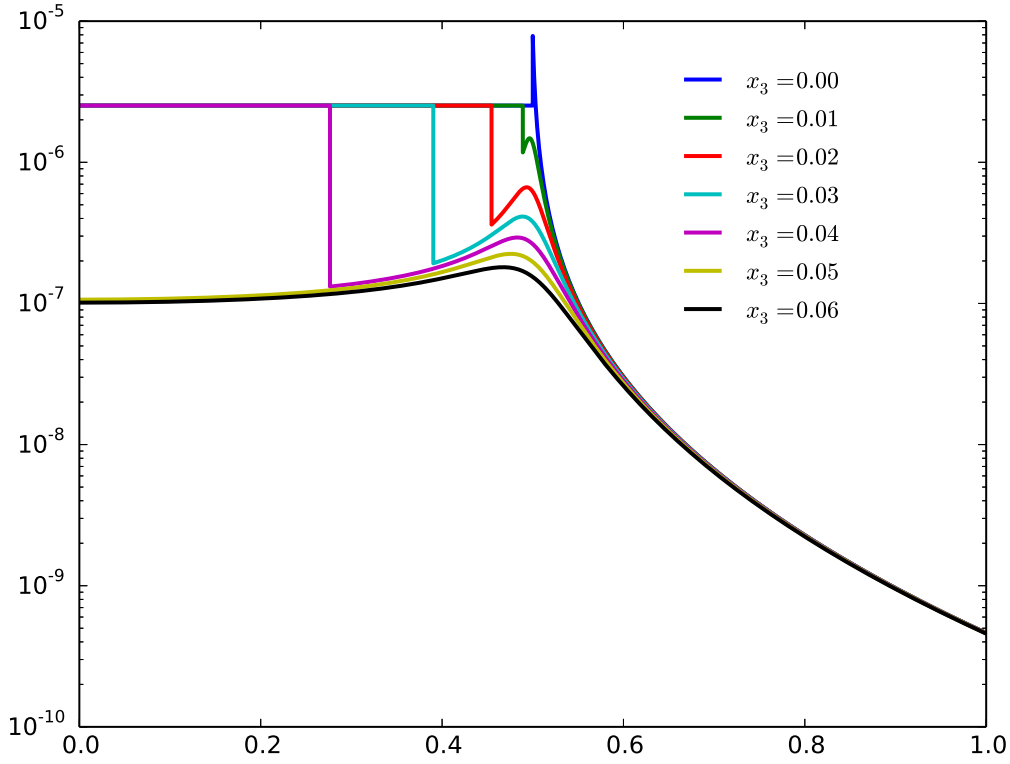

Figure 3: Oblate ellipsoid; energy density versus x_1, $x_2 = 0$

5.2 Oblate size study: energy and pressure calculations

In this section, energy calculations for oblate inclusions with varying size and aspect ratios are presented; for selected cases, pressure in and around inclusions is graphically illustrated; material properties used for these calculations are given in Table 2.

Using formulas given in Section 4.1, the total elastic energy in the matrix and inclusion are given in Table 6 for oblate inclusions with aspect ratios of 2:1, 3:1 and 5:1 and ranging in size from 0.2 microns to 0.5 microns in the major direction. There are perhaps two obvious observations that can be made from this table:

1. For a given aspect ratio, the energy density on inclusion is constant and independent of inclusion size.

2. Fraction of elastic energy stored in matrix tends to be higher for oblate inclusions with smaller aspect ratios – for example, compare first row with last row in Table 6.

In some applications, it may be useful to identify regions near and around an inclusion where the trace of the stress tensor is positive, .i.e. tensile stress components exist at the point in

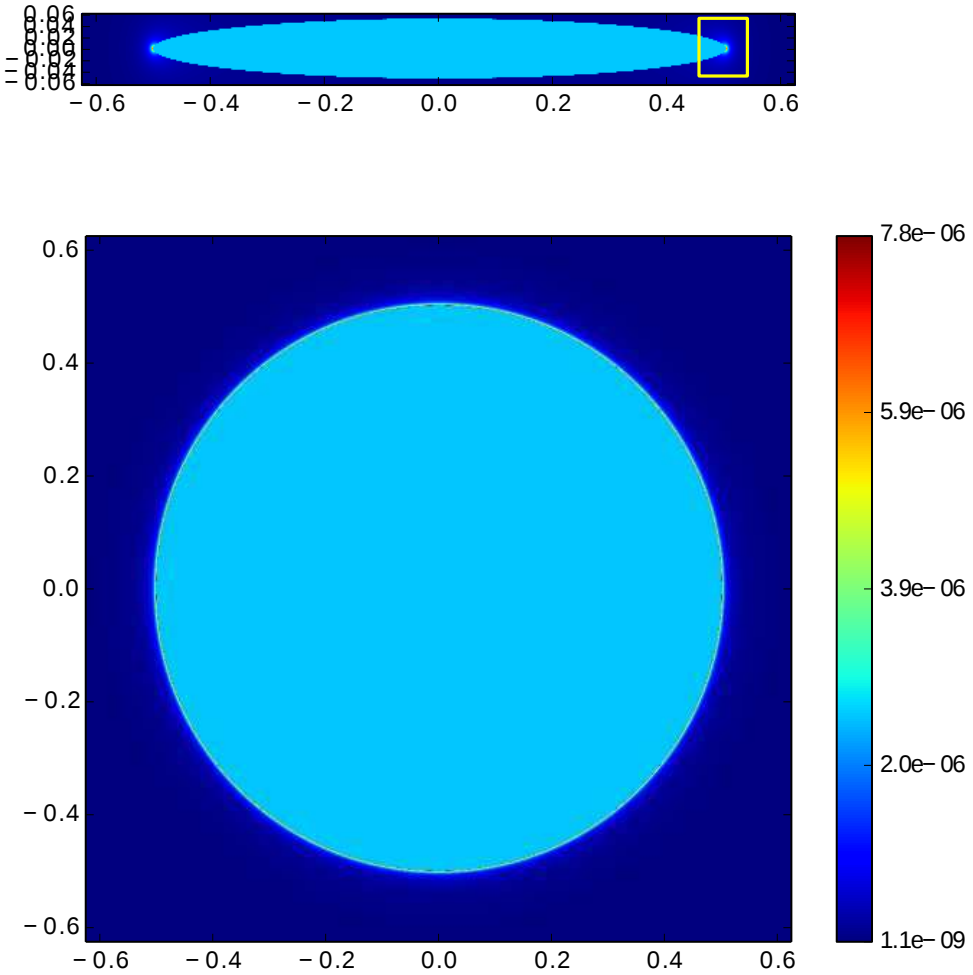

Figure 4: Oblate ellipsoid; energy density sections; upper graphic '$x_1 - x_3$' plane at $x_2 = 0$, lower graphic '$x_1 - x_2$' plane at $x_3 = 0$.

question. Components of the stress tensor at a point are evaluated using the *Eshelby* library and then the scalar $p = \frac{1}{3}(\sigma_{xx} + \sigma_{yy} + \sigma_{zz})$ is computed as a post-processing step. One case (a_1, a_2, a_3)=(0.500, 0.500, 0.100), taken from Table 6, is shown in Figures 11 and 12, where for plotting purposes, p is set to zero wherever $p < 0$ in Figure 11; the exact magnitudes of pressure shown can be taken from Figure 12 where the blue curve corresponds with the plane depicted in Figure 11. Note that the dark blue interior of the inclusion is under compression and casts a shadow; tension is shown in the colored regions around the edge of the inclusion.

5.3 Computations on inclusions with extreme aspect ratio

A reviewer inquired as to what happens numerically when the aspect ratio of an inclusion becomes very large. This topic is briefly presented using calculations on an oblate inclusion.

Consider the case $a_1 = a_2 = 100.0$, where $a_3 = a_1/h$ is calculated using the following sequence of

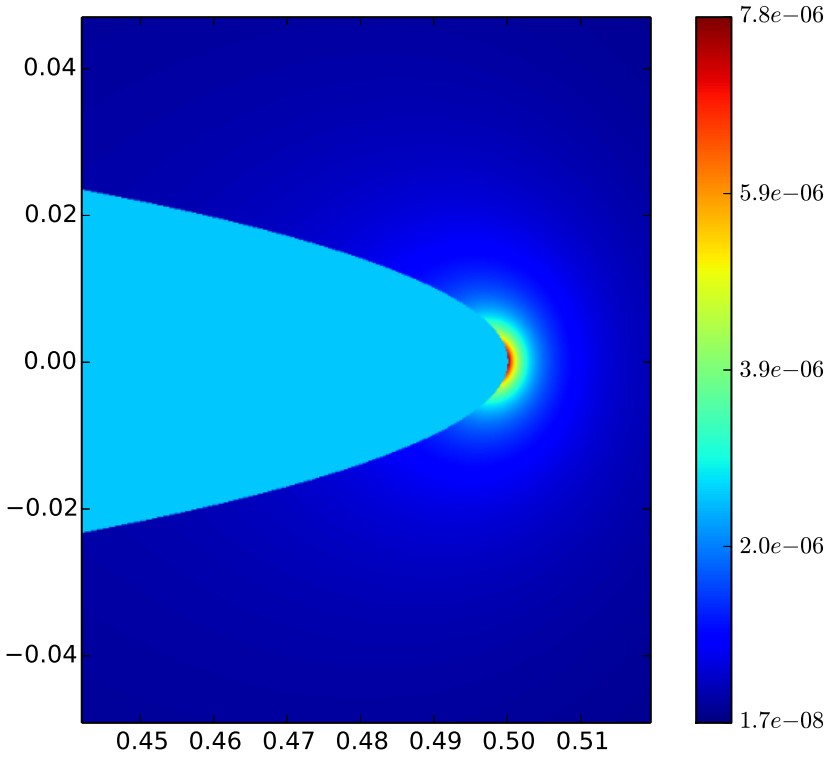

Figure 5: Oblate ellipsoid; energy density; zoom window shown in Figure 4.

aspect ratios: $h = 5, 10, 1000, 10000, 100000, 1000000, 10000000$; note that this sequence produces extremely thin inclusions which in some cases may go beyond what is physically realistic with respect to the units used. Nonetheless, these simulations are useful in demonstrating the strengths and weaknesses of the numerical implementation; results for some of these cases are shown in Table 7 and Figures 13 and 14. Note that as the aspect ratio increases, the energy density on the inclusion reaches a limiting value of 3.32×10^{-12} while the relative amount of energy stored in the matrix decreases dramatically. Although there is a small decrease in the magnitude of pressure as aspect ratio increases, pressure on the interior of the inclusion is relatively insensitive to both size and aspect ratio; as the aspect ratio increases, the pressure looks like a step function rising from a uniform value of compression on the interior to a value of 0.0 just outside the inclusion. However, when $a_1 = a_2 = .5$, the calculation $(h = 10000000, h = a_1/a_3)$ fails on the pressure plot (see Figures 12 and 15) although the energy density calculation succeeds; see Table 8 and note that both energy density and pressure are visually nearly identical for cases $a_1 = a_2 = 100$ and $a_1 = a_2 = .5$ – apparently both energy and pressure on the interior of the inclusion only depend upon the aspect ratio.

Based upon these calculations, it is hypothesized that as aspect ratios increase, there is some size dependent round-off sensitivity for calculations at exterior points. Energy calculations (which didn't fail) only require calculation of the Eshelby tensor S_{ijkl} for interior points ($\lambda = 0$) whereas

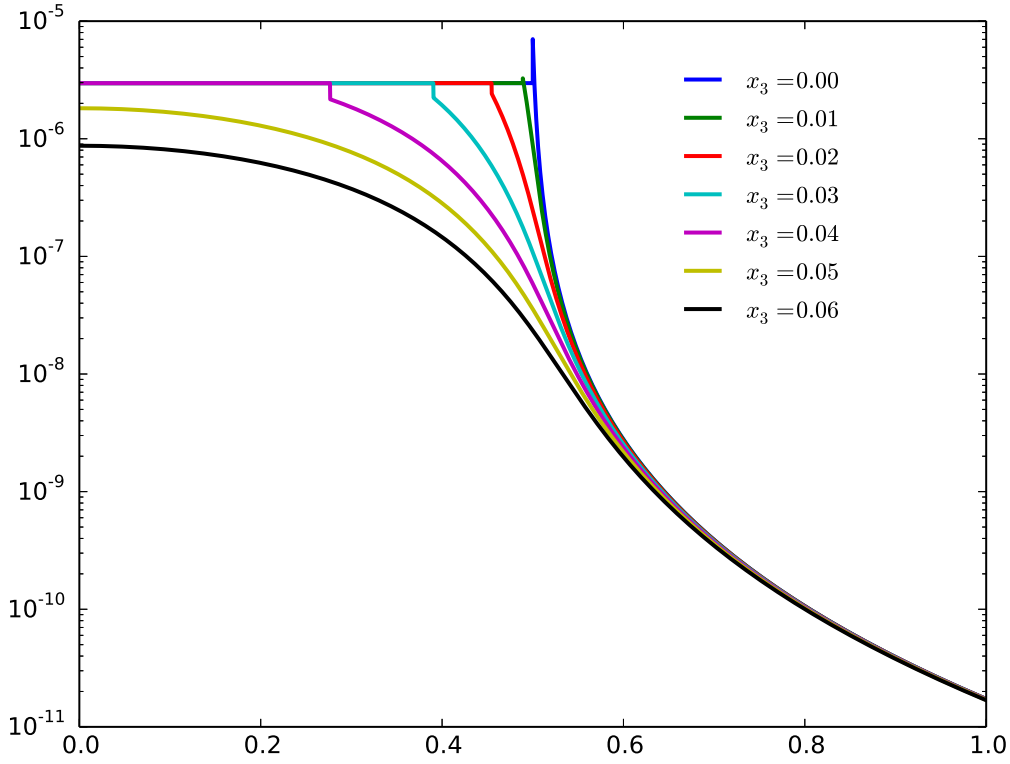

Figure 6: Prolate ellipsoid; energy density versus x_1, $x_2 = 0$

exterior points ($\lambda ! = 0$) require calculation of D. Nonetheless, these calculations demonstrate the ability of the *Eshelby* library to resolve complex elastic fields in and around inclusions with extreme aspect ratios.

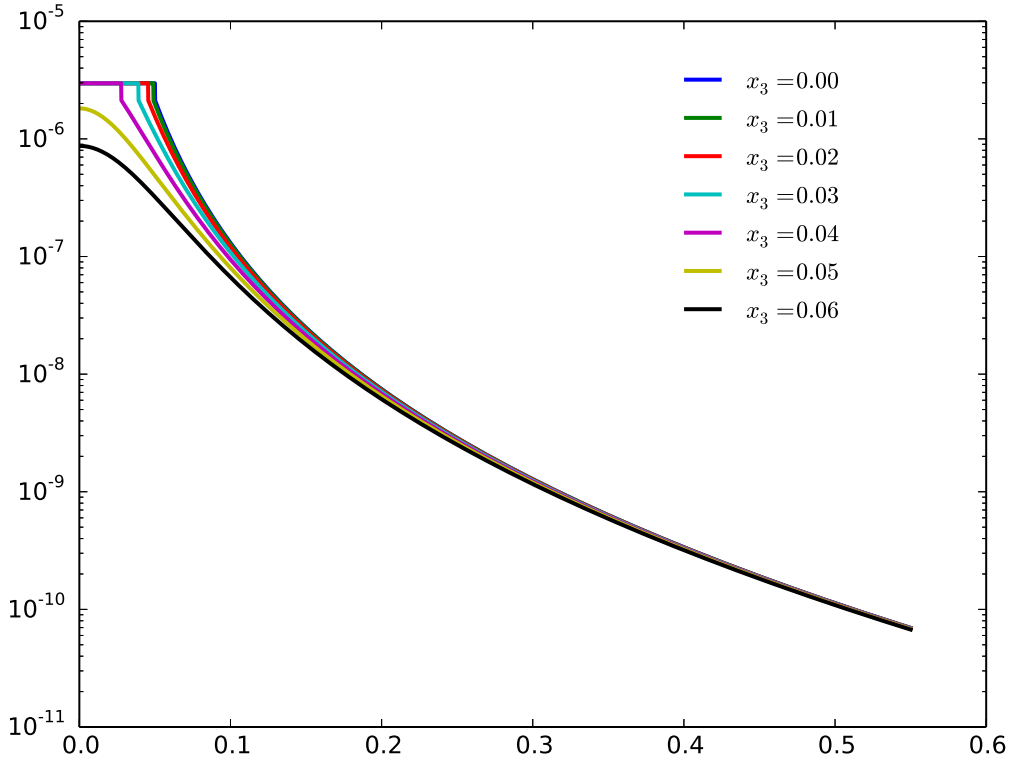

Figure 7: Prolate ellipsoid; energy density versus x_2, $x_1 = 0$

Table 6: Size study on oblate inclusions including fixed aspect ratios. Units: size (microns), volume (cubic microns), energy density (Joules per cubic micron), energy (Joules); See Table 2 for moduli used in these calculations.

Size	*Inclusion*			*Matrix*	*Total*
(a_1, a_2, a_3)	*volume*	*energy density*	*energy*	*energy*	*energy*
$(0.200, 0.200, 0.100)$	0.017	1.45×10^{-12}	2.43×10^{-14}	4.61×10^{-14}	7.04×10^{-14}
$(0.300, 0.300, 0.150)$	0.057	1.45×10^{-12}	8.21×10^{-14}	1.56×10^{-13}	2.38×10^{-13}
$(0.400, 0.400, 0.200)$	0.134	1.45×10^{-12}	1.95×10^{-13}	3.69×10^{-13}	5.63×10^{-13}
$(0.500, 0.500, 0.250)$	0.262	1.45×10^{-12}	3.80×10^{-13}	7.20×10^{-13}	1.10×10^{-12}
$(0.200, 0.200, 0.067)$	0.011	1.65×10^{-12}	1.85×10^{-14}	2.61×10^{-14}	4.46×10^{-14}
$(0.300, 0.300, 0.100)$	0.038	1.65×10^{-12}	6.24×10^{-14}	8.82×10^{-14}	1.51×10^{-13}
$(0.400, 0.400, 0.133)$	0.089	1.65×10^{-12}	1.48×10^{-13}	2.09×10^{-13}	3.57×10^{-13}
$(0.500, 0.500, 0.167)$	0.175	1.65×10^{-12}	2.89×10^{-13}	4.08×10^{-13}	6.97×10^{-13}
$(0.200, 0.200, 0.040)$	0.007	2.03×10^{-12}	1.36×10^{-14}	1.17×10^{-14}	2.53×10^{-14}
$(0.300, 0.300, 0.060)$	0.023	2.03×10^{-12}	4.59×10^{-14}	3.96×10^{-14}	8.54×10^{-14}
$(0.400, 0.400, 0.080)$	0.054	2.03×10^{-12}	1.09×10^{-13}	9.38×10^{-14}	2.02×10^{-13}
$(0.500, 0.500, 0.100)$	0.105	2.03×10^{-12}	2.12×10^{-13}	1.83×10^{-13}	3.96×10^{-13}

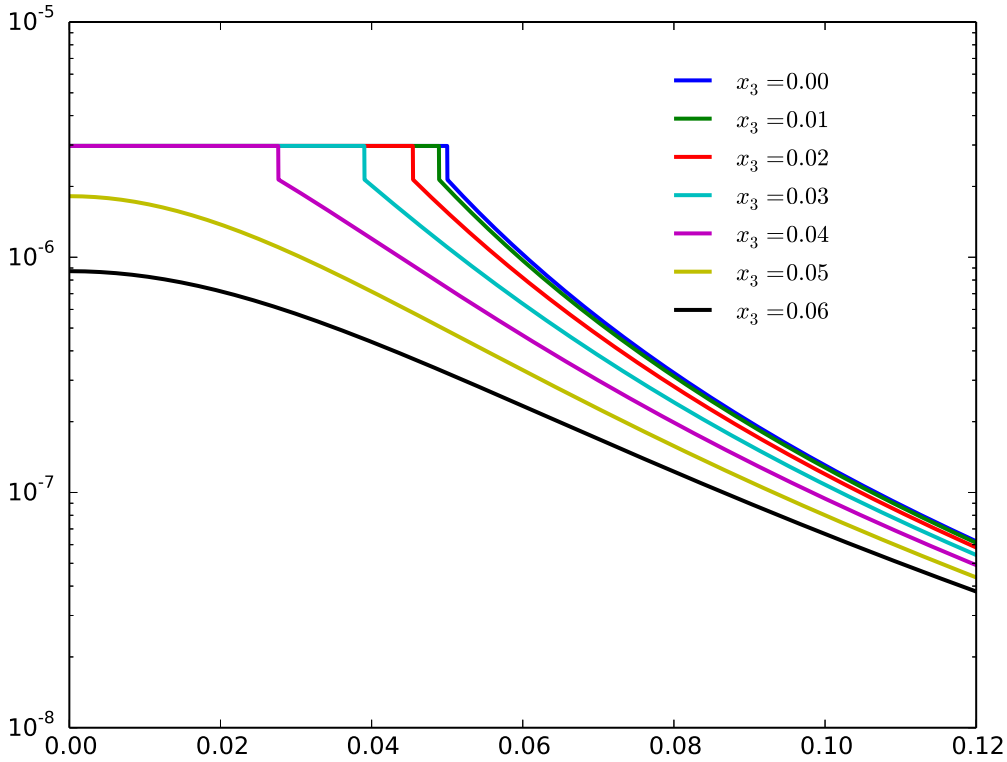

Figure 8: Prolate ellipsoid; energy density versus zoomed x_2, $x_1 = 0$

Table 7: Study on extreme-aspect-ratio oblate inclusions. Units: size (microns), volume (cubic microns), energy density (Joules per cubic micron), energy (Joules); See Table 2 for moduli used in these calculations; $a_1 = a_2 = 100, a_3 = a_1/h$.

Aspect ratio	*Inclusion*			*Matrix*	*Total*
h	*volume*	*energy density*	*energy*	*energy*	*energy*
5×10^{0}	8.38×10^{5}	2.03×10^{-12}	1.70×10^{-06}	1.47×10^{-06}	3.16×10^{-06}
1×10^{1}	4.19×10^{5}	2.52×10^{-12}	1.06×10^{-06}	4.39×10^{-07}	1.50×10^{-06}
1×10^{2}	4.19×10^{4}	3.22×10^{-12}	1.35×10^{-07}	5.25×10^{-09}	1.40×10^{-07}
1×10^{3}	4.19×10^{3}	3.31×10^{-12}	1.38×10^{-08}	5.35×10^{-11}	1.39×10^{-08}
1×10^{4}	4.19×10^{2}	3.32×10^{-12}	1.39×10^{-09}	5.36×10^{-13}	1.39×10^{-09}
1×10^{5}	4.19×10^{1}	3.32×10^{-12}	1.39×10^{-10}	5.36×10^{-15}	1.39×10^{-10}
1×10^{6}	4.19×10^{0}	3.32×10^{-12}	1.39×10^{-11}	5.36×10^{-17}	1.39×10^{-11}
1×10^{7}	4.19×10^{-1}	3.32×10^{-12}	1.39×10^{-12}	5.36×10^{-19}	1.39×10^{-12}

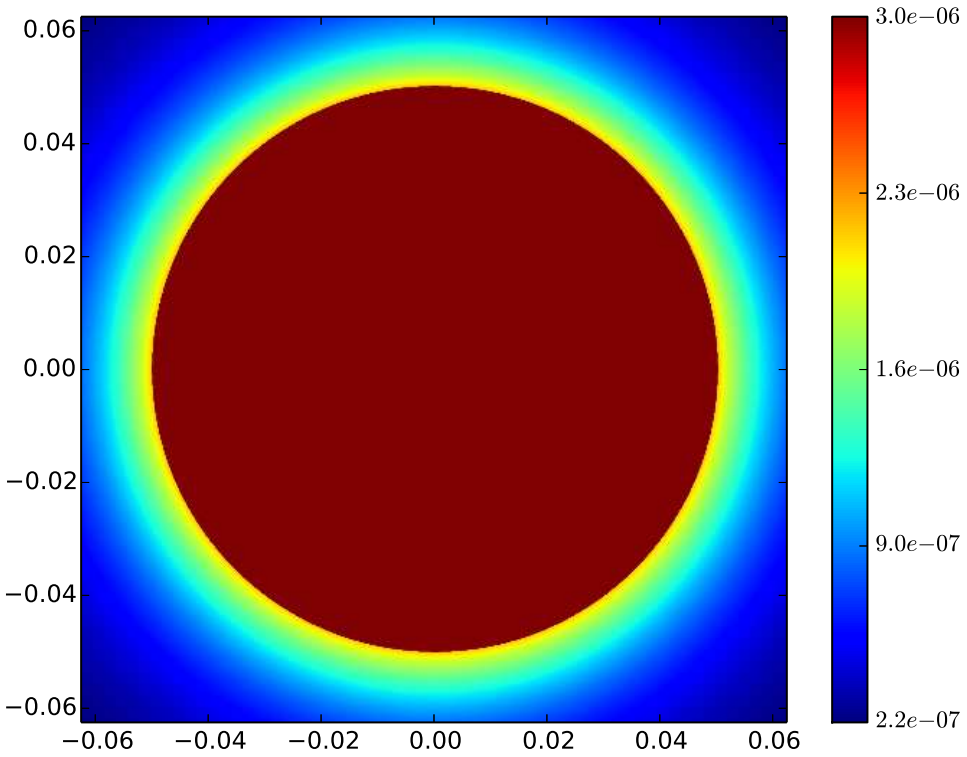

Figure 9: Prolate ellipsoid; energy density sections; '$x_2 - x_3$' plane at $x_1 = 0$.

Table 8: Study on extreme-aspect-ratio oblate inclusions. Units: size (microns), volume (cubic microns), energy density (Joules per cubic micron), energy (Joules); See Table 2 for moduli used in these calculations; $a_1 = a_2 = 0.5, a_3 = a_1/h$.

Aspect ratio	*Inclusion*			*Matrix*	*Total*
h	*volume*	*energy density*	*energy*	*energy*	*energy*
5×10^{0}	1.05×10^{-01}	2.03×10^{-12}	2.12×10^{-13}	1.83×10^{-13}	3.96×10^{-13}
1×10^{1}	5.24×10^{-02}	2.52×10^{-12}	1.32×10^{-13}	5.49×10^{-14}	1.87×10^{-13}
1×10^{2}	5.24×10^{-03}	3.22×10^{-12}	1.69×10^{-14}	6.56×10^{-16}	1.75×10^{-14}
1×10^{3}	5.24×10^{-04}	3.31×10^{-12}	1.73×10^{-15}	6.68×10^{-18}	1.74×10^{-15}
1×10^{4}	5.24×10^{-05}	3.32×10^{-12}	1.74×10^{-16}	6.70×10^{-20}	1.74×10^{-16}
1×10^{5}	5.24×10^{-06}	3.32×10^{-12}	1.74×10^{-17}	6.70×10^{-22}	1.74×10^{-17}
1×10^{6}	5.24×10^{-07}	3.32×10^{-12}	1.74×10^{-18}	6.70×10^{-24}	1.74×10^{-18}
1×10^{7}	5.24×10^{-08}	3.32×10^{-12}	1.74×10^{-19}	6.70×10^{-26}	1.74×10^{-19}

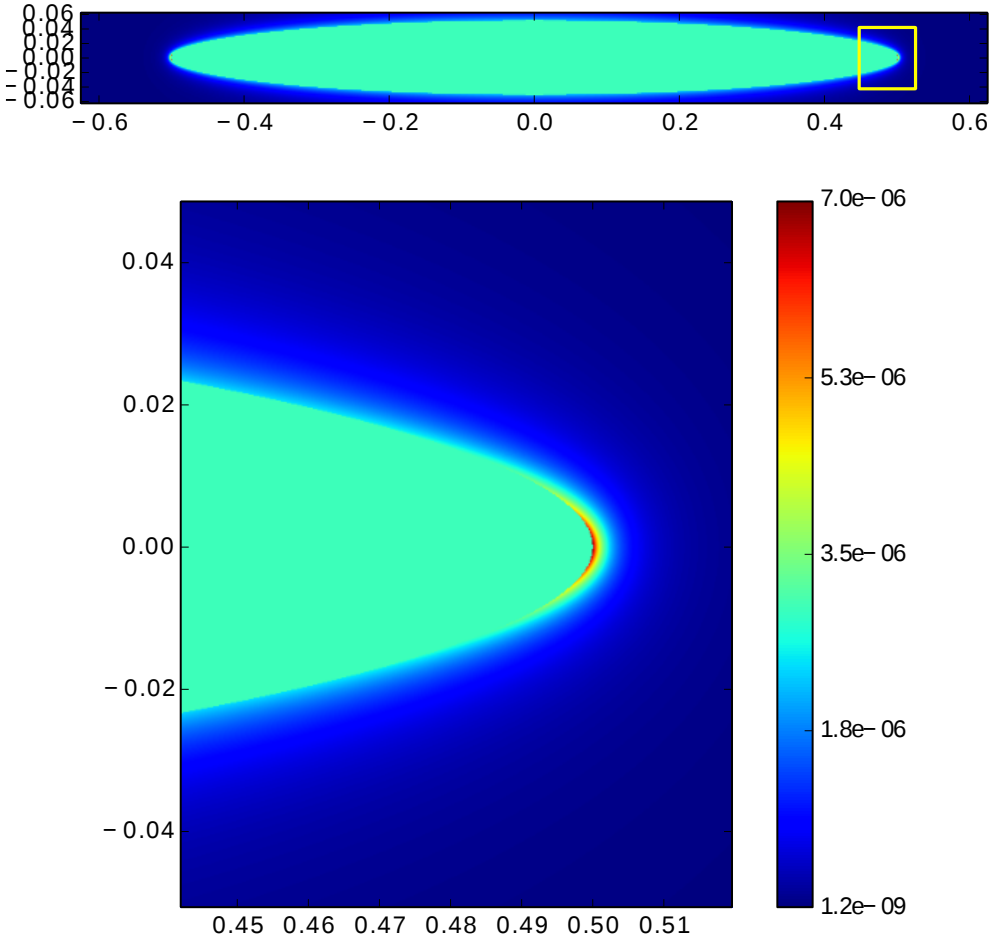

Figure 10: Prolate ellipsoid; energy density; top '$x_1 - x_3$' plane at $x_2 = 0$, bottom zoom window.

Figure 11: Pressure p on oblate ellipsoid in $x_1 - x_3$ plane at $x_2 = 0$.

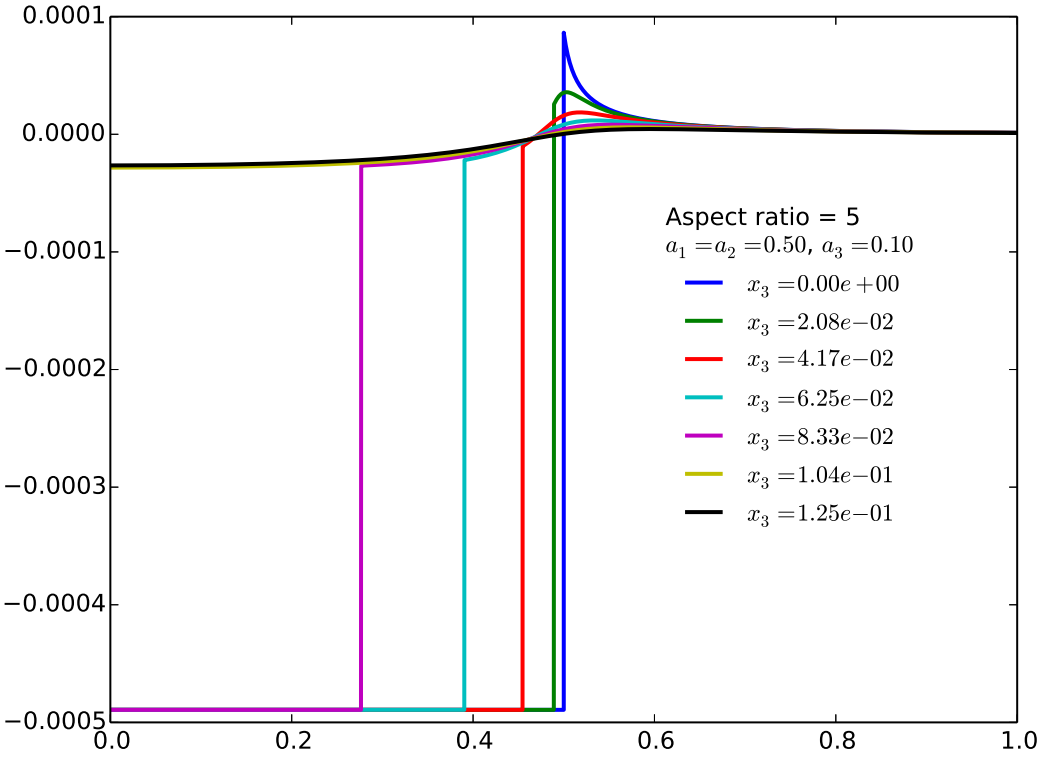

Figure 12: Oblate ellipsoid ($a_1 = a_2 = 0.5, a3 = a_1/h$, $h = 5$); pressure p versus x_1.

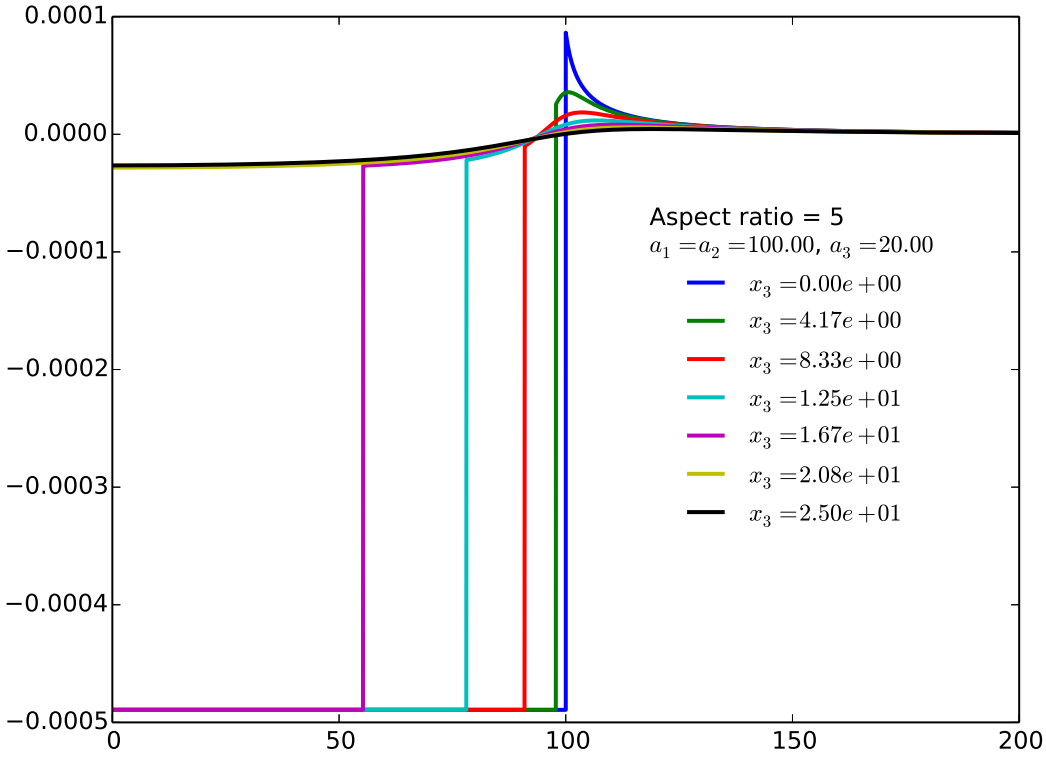

Figure 13: Oblate ellipsoid ($a_1 = a_2 = 100.0, a3 = a_1/h$, $h = 5$); pressure p versus x_1.

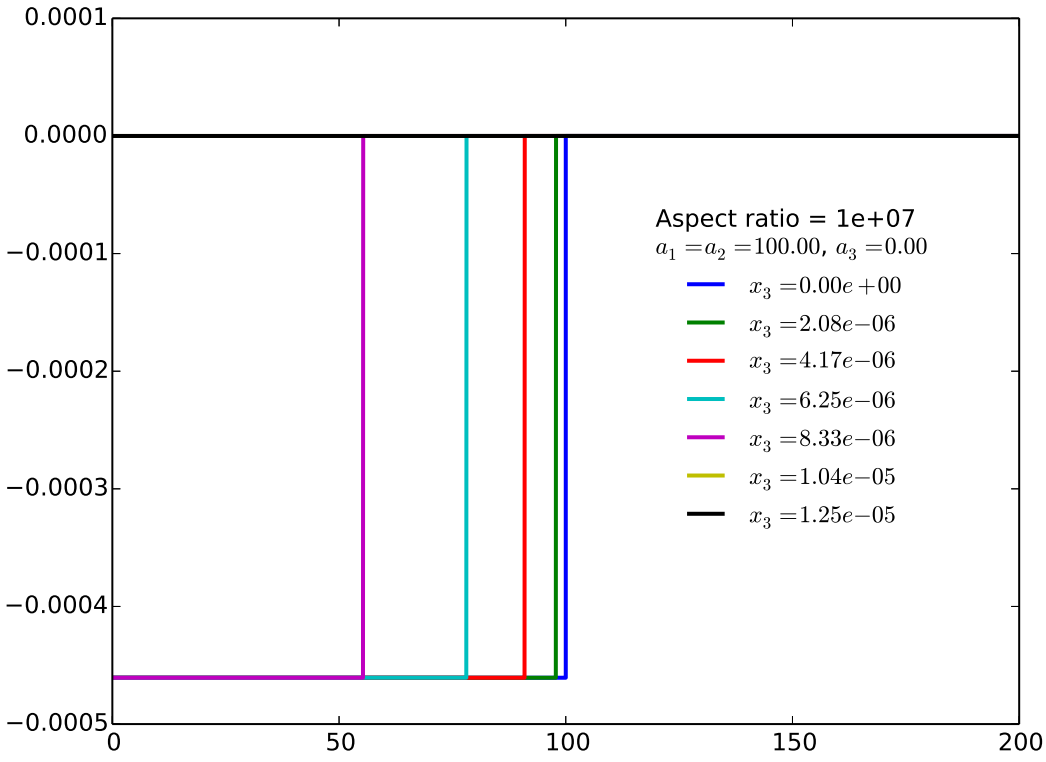

Figure 14: Oblate ellipsoid ($a_1 = a_2 = 100.0, a3 = a_1/h$, $h = 1 \times 10^7$); pressure p versus x_1.

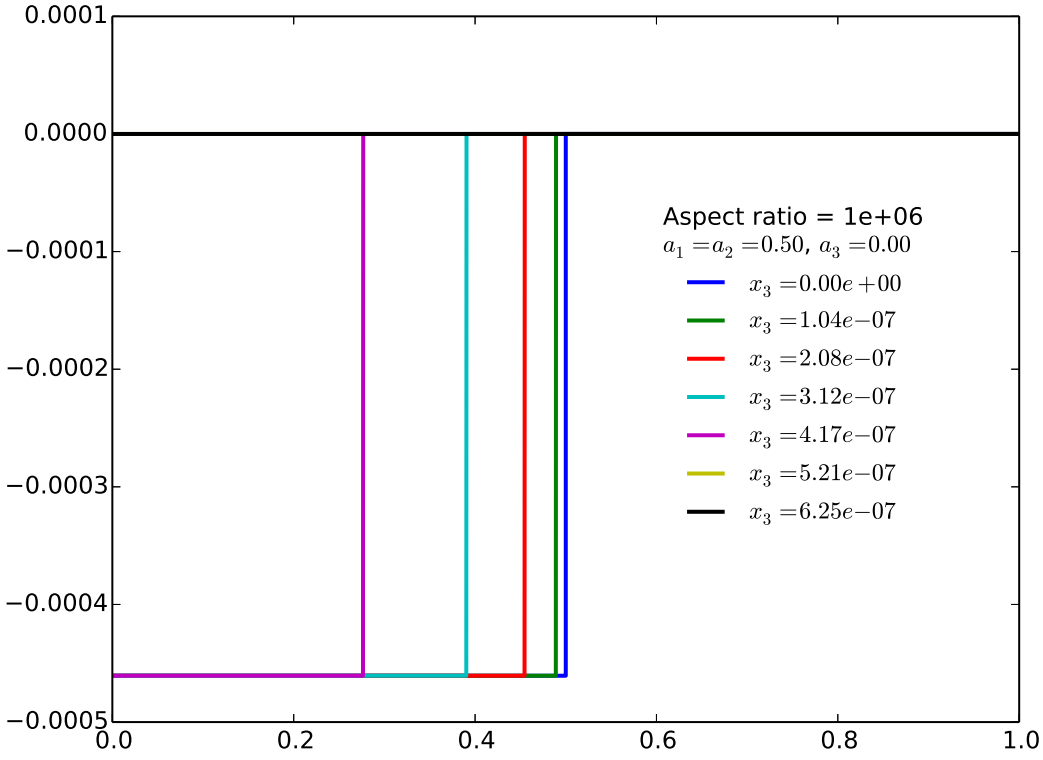

Figure 15: Oblate ellipsoid ($a_1 = a_2 = 0.5, a3 = a_1/h$, $h = 1 \times 10^6$); pressure p versus x_1.

6 Summary

The mathematical formulas implemented in the *Eshelby* library were documented in this report; some demonstration calculations using the library were also presented. The library can be used to calculate strain, stress and energy density in and around isotropic inclusions making it a valuable tool for kinetic models of precipitate formation where elastic energy may play an important role. Calculations show remarkable resolution of stress and energy density near the surface of inclusions that would otherwise be very difficult to resolve with routine finite element calculations; demonstration calculations show that this is even true for inclusions with extreme aspect ratios suggesting the use of the *Eshelby* library for resolving elastic fields around cracks. The library is written in c++ and is very extensible, especially for generalized ellipsoids, and in-homogeneous inclusions and the equivalent inclusion method.

References

[1] J. D. Eshelby, "The determination of the elastic field of an ellipsoidal inclusion, and related problems," *Proc. R. Soc. A*, vol. 241, pp. 376–396, 1957.

[2] T. Mura, *Micromechanics of Defects in Solids*, 2nd ed. Kluwer Academic Publishers, 1987.

[3] C. Meng, W. Heltsley, and D. D. Pollard, "Evaluation of the Eshelby solution for the ellipsoidal inclusion," *Computers and Geosciences*, vol. 40, pp. 40–48, 2012.

[4] W. R. Inc., *Mathematica*, version 9.0 ed. Wolfram Research, Inc., 2014.

[5] *GNU Scientific Library Reference Manual*, version 1.16, http://www.gnu.org/software/gsl/.

1 Partial derivatives of I-integrals

The final form of the Eshelby tensor in (16) is obtained using (10) and (19); however, note that multiple partial derivatives of $\phi(\mathbf{x})$ and $\psi(\mathbf{x})$ are required. The integrals in (12) only depend upon $\mathbf{x}$ through the lower limit λ; the upper limit (∞) is independent of $\mathbf{x}$. Using the Leibniz integral rule, partial derivatives of the I-integrals in (12) are evaluated and depend upon expressions for $\lambda_{,j}$ and $\lambda_{,jk}$ given in Appendix 2.

$$I_{,j} = -\frac{2\pi a_1 a_2 a_3}{\Delta(\lambda)}\lambda_{,j} \tag{45}$$

Partial derivatives $I_{i\ldots jk,p}$ and expressions of the form $x_n x_n I_{N,j}$ are facilitated and verified using the following relations [2]

$$I_{i\ldots jk,p} = \frac{1}{a_K^2+\lambda} I_{i\ldots j,p}, \quad x_n x_n I_{N,j} = \left(\frac{x_n x_n}{a_N^2+\lambda}\right) I_{,j} = I_{,j}, \tag{46}$$

where the last equality in the above uses (14).

The partial derivatives $I_{i,j}$ and $I_{i,jk}$ are evaluated; the expressions obtained were published by Meng, Heltsley, and Pollard [3] in 2012. Note that the integral for I_i in (12) only depends upon $\mathbf{x}$ through the lower limit λ. Using the Leibniz integral rule, the partial derivative $I_{I,j}$ is evaluated as

$$I_{I,j} = -2\pi a_1 a_2 a_3 \left(\frac{1}{(a_I^2+\lambda)}\frac{1}{\Delta(\lambda)}\right)\lambda_{,j} = \frac{1}{(a_I^2+\lambda)} I_{,j}, \tag{47}$$

where the second equality above can be obtained by inspection using (45) or by applying the first relation in (46). Towards evaluating $I_{i,jk}$, the partial derivative of the term in parentheses above is

$$\frac{\partial}{\partial x_k}\left[\frac{1}{(a_I^2+\lambda)}\frac{1}{\Delta(\lambda)}\right] = -\frac{\lambda_{,k}}{(a_I^2+\lambda)^2}\frac{1}{\Delta(\lambda)} - \frac{1}{(a_I^2+\lambda)}\frac{1}{\Delta(\lambda)^2}\frac{\partial\Delta}{\partial x_k},$$

where

$$\begin{aligned}\frac{1}{\Delta(\lambda)^2}\frac{\partial\Delta}{\partial x_k} &= \frac{1}{2\Delta}\left[(a_2^2+\lambda)(a_3^2+\lambda)+(a_1^2+\lambda)(a_3^2+\lambda)+(a_1^2+\lambda)(a_2^2+\lambda)\right]\lambda_{,k} \\ &= \frac{1}{2\Delta(\lambda)}\left[\frac{1}{a_1^2+\lambda}+\frac{1}{a_2^2+\lambda}+\frac{1}{a_3^2+\lambda}\right]\lambda_{,k}.\end{aligned} \tag{48}$$

Using the product rule and the above two expressions,

$$I_{I,jk} = \frac{-2\pi a_1 a_2 a_3}{(a_I^2+\lambda)\Delta(\lambda)}\left[\lambda_{,jk} - \lambda_{,j}\lambda_{,k}\left(\frac{1}{a_I^2+\lambda}+\frac{1}{2}\left(\frac{1}{a_1^2+\lambda}+\frac{1}{a_2^2+\lambda}+\frac{1}{a_3^2+\lambda}\right)\right)\right]. \tag{49}$$

The integral for I_{IJ} in (12) only depends upon $\mathbf{x}$ through the lower limit λ. Using the Leibniz integral rule, the partial derivative $I_{IJ,k}$ is evaluated as

$$I_{IJ,k} = -\frac{2\pi a_1 a_2 a_3}{(a_I^2+\lambda)(a_J^2+\lambda)\Delta(\lambda)}\lambda_{,k}. \tag{50}$$

The partial derivative of the denominator term in the above is given by

$$\frac{\partial}{\partial x_l}\left[\frac{1}{(a_I^2+\lambda)(a_J^2+\lambda)\Delta(\lambda)}\right] = -\frac{\lambda_{,l}}{(a_I^2+\lambda)^2(a_J^2+\lambda)\Delta(\lambda)} - \frac{\lambda_{,l}}{(a_I^2+\lambda)(a_J^2+\lambda)^2\Delta(\lambda)} - \frac{1}{(a_I^2+\lambda)(a_J^2+\lambda)}\frac{1}{\Delta(\lambda)^2}\frac{\partial\Delta}{\partial x_k}.$$

Using the product rule, (48), and above expression, $I_{IJ,kl}$ is given as

$$I_{IJ,kl} = \frac{-2\pi a_1 a_2 a_3}{(a_I^2+\lambda)(a_J^2+\lambda)\Delta(\lambda)}\left[\lambda_{,kl} - \left(\frac{1}{a_I^2+\lambda}+\frac{1}{a_J^2+\lambda}+\frac{1}{2}\left(\frac{1}{a_1^2+\lambda}+\frac{1}{a_2^2+\lambda}+\frac{1}{a_3^2+\lambda}\right)\right)\lambda_{,k}\lambda_{,l}\right].$$

2 Partial derivatives of λ

There is an explicit dependence of $\phi(\mathbf{x})$ and $\psi(\mathbf{x})$ on the coordinates x_i in (19) and an implicit dependence through λ in the I-integrals (12). Partial derivatives of λ are derived beginning with (14).

$$\lambda_{,i} = \frac{F_i}{a_I^2+\lambda}, \qquad \lambda_{,ik} = \frac{F_{i,k} - \lambda_{,i}C_{,k}}{C},$$

where

$$F_i = \frac{2x_i}{a_I^2+\lambda}, \qquad F_{i,k} = \frac{2\delta_{ik}}{a_I^2+\lambda} - \frac{F_i}{a_I^2+\lambda}\lambda_{,k}, \qquad C = \frac{x_j x_j}{(a_J^2+\lambda)^2}, \qquad C_{,k} = \frac{F_k}{(a_K^2+\lambda)} - \frac{2x_j x_j}{(a_J^2+\lambda)^3}\lambda_{,k}.$$

DISTRIBUTION:

1 MS 0899 RIM-Reports Management, 9532 (electronic copy)


Sandia National Laboratories